



Ethanol Gas Sensor Fabrication Based on ZnO Flower Like Nanorods

Abdulqader D. Faisal ^{id}^a, Mofeed A. Jaleel ^b, Fahad Z. Kamal ^{c*}

^a Department of Applied Sciences, University of Technology, Baghdad, Iraq. Email: abdulf330@yahoo.com

^b Department of Applied Sciences, University of Technology, Baghdad, Iraq.

^c Department of Applied Sciences, University of Technology, Baghdad, Iraq.

*Corresponding author.

Submitted: 04/05/2019

Accepted: 01/09/2020

Published: 25/12/2020

KEY WORDS

Hydrothermal, flower-like, ZnO NRs, ethanol gas sensors, activation energy.

ABSTRACT

Zinc oxide flower-like nanorods (ZnO NRs) was successfully synthesized via the hydrothermal method. The growth process was conducted with seed layer concentrations of 20mM. The as-synthesized nanostructures were characterized by x-ray diffraction (XRD), scanning electron microscope (SEM), atomic force microscope (AFM), and ultraviolet-visible (UV-VIS) spectrophotometer. The analysis results revealed a pure Wurtzite ZnO hexagonal nanostructures with preferred orientation (002) along the c-direction. The calculated band gap of average crystallite size is 3.2eV and 25 nm respectively. New designed, constructed and successfully calibrated for ethanol gas sensing was found. The ethanol gas sensor was fabricated at room temperature based on the ZnO NRs film. The synthesized materials proved to be a good candidate for the ethanol gas sensor. The optimum results of the gas sensor measurements of the synthesized gas sensor are as follows, the sensitivity, response time, and recovery time at 25 °C are 60%, 80 Seconds and 80 seconds respectively, and at 200 °C are 70%, 60 seconds and 50 seconds respectively.

How to cite this article: A. D. Faisal, M. A. Jaleel and F. Z. Kamal, "Ethanol Gas Sensor Fabrication Based on ZnO Flower Like Nanorods," Engineering and Technology Journal, Vol. 38, Part B, No. 03, pp. 85-97, 2020.

DOI: <https://doi.org/10.30684/etj.v38i3B.279>

This is an open access article under the CC BY 4.0 license <http://creativecommons.org/licenses/by/4.0>.

1. INTRODUCTION

Zinc oxide (ZnO) is a very attractive semiconductor [1], because it has a very wide direct band gap of 3.37 eV at ambient conditions [2], and it also possesses a free exciton binding energy of 60 meV [3]. It is currently used for advanced technologies and industries due to its extraordinary transparency [4]. Due to the extremely superior properties, it was employed for the production of efficient solar cells [5], light-emitting diodes [6], piezoelectric devices [7], and transparent leads [8], chemical sensors [9], gas sensors [10-12]. Recently lots of techniques were developed for the

synthesis of zinc oxide such as aqueous thermal decomposition [13], microwave activated chemical bath deposition (MACBD) [14], chemical bath deposition (CBD) [15], vapor-liquid-solid (VLS) growth [16], metal-organic catalyst assisted vapor phase growth (MOCVPG) [17], Chemical vapor deposition (CVD) [18,19], and direct evaporation [20]. The above methods are somehow expensive and complex, therefore other routes were investigated such as hydrothermal synthesis for the preparation of transparent semiconducting oxides [21]. The hydrothermal method is less expensive and simple [22,23], and it can be worked at low temperatures ($>90^{\circ}\text{C}$) [24]. Recently ZnO has been considered as a favorable material for redox gas sensors because of its high electrochemical stability, non-toxic, suitability to doping, and low cost [25]. The sensing capabilities of a sensor depend mainly on the shape and morphologies of the sensing material, so that many morphologies of ZnO nanostructures have been synthesized and studied. Researches have shown that one-dimensional (1D) ZnO nanostructures possess a large surface-to-volume ratio, which can adsorb more molecules on the sensing surface [26-32]. Various morphologies can be synthesized via different techniques such as nanorods [33], nanowires [34], nanoflowers [35], comb-like [36], and nanowalls [37].

The objective of this work is the synthesis of ZnO NRs (Flower-like nanorods) via hydrothermal technique and the design, construction and calibration of the new gas-sensor system. The synthesized material was fabricated as an ethanol gas sensor. The gas sensing performance was investigated using 500 ppm of ethanol vapor concentration at substrate temperatures of 25°C and 200°C .

2. EXPERIMENTAL PART

I. Silicon substrate cleaning

Before the synthesis process, (100) p-type silicon wafers were cut into (100 mm²) substrates and cleaned with deionized water, propanol and acetone, by immersing the substrate in each reagent for 15 min under an ultrasonic bath at 50°C after each immersion the substrates were blown with nitrogen gun, this procedure was repeated three times.

II. Seed layer preparation

Seed layer solution was prepared by dissolving a concentration of 20mM of zinc acetate ($\text{Zn}(\text{CH}_3\text{COO})_2 \cdot 2\text{H}_2\text{O}$) in 10 ml ethyl alcohol and ultrasonication of the solution for 30 minutes, afterward, a drop-casting method was utilized in order to coat the substrates with a seed layer solution using a micropipette. After each coating, the substrate was dried using N_2 gas, the coating was repeated 5 times. Then the seeded substrates were heat treated at 500°C for one hour in a home-made tube furnace, in order to evaporate water molecules, organic matters burn off and to induce some crystalline. These ZnO nanocrystals would act as nucleation sites for the growth of ZnO nanostructures.

III. Hydrothermal growth

The growth solution was prepared by dissolving 25 mM zinc nitrate hexahydrate ($\text{Zn}(\text{NO}_3)_2 \cdot 6\text{H}_2\text{O}$) and 25 mM hexamethylenetetramine (HMTA) in DI water in a 100mL glass beaker, and the solution was sonicated for 60 minutes to ensure full dissolution of the precursors. The prepared growth solution was then transferred to the Homemade glass cell with a volume of 150 mL that used to perform hydrothermal growth. The pre-seeded substrates were fixed upside down inside the growth solution using a homemade Teflon holder as shown in Fig.1. This cell is transferred into a laboratory oven and the samples were heated at 90°C for 2h. After growth, the cell was removed from the oven and rinsed thoroughly with DI water to remove any residual reactants and dried in air at normal atmosphere. The grown substrates were subsequently annealed using a programmable muffle furnace at 500°C for 1h in order to remove the organic materials and decompose the zinc acetate to form ZnO nanocrystals.

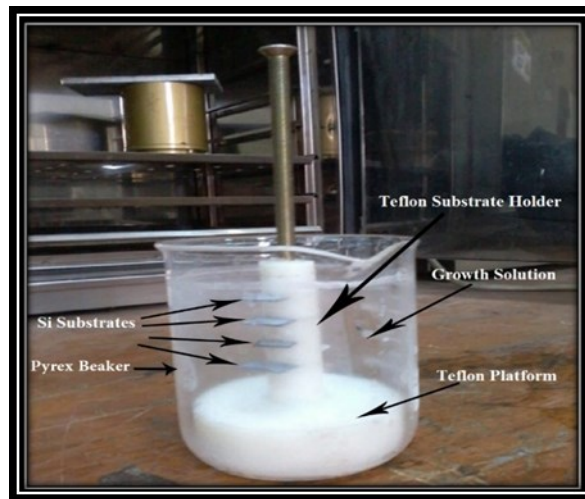


Figure 1: Photograph of the home-made hydrothermal growth, the cell with the silicon substrates.

3. RESULTS AND DISCUSSION

I. Atomic Force Microscopy (AFM) Analysis

The seed layer of ZnO nanocrystals at concentrations of acetate solution of 20mM was analyzed via the AFM technique. The 2D, 3D images and the granularity distribution of ZnO of these concentrations are shown in Fig. 2. The amplitude parameters from the AFM data for ZnO nanorods are average grain size, Sa (Roughness Average), and Sq (Root mean square) 95.85, 1.7nm, and 1.96nm respectively.

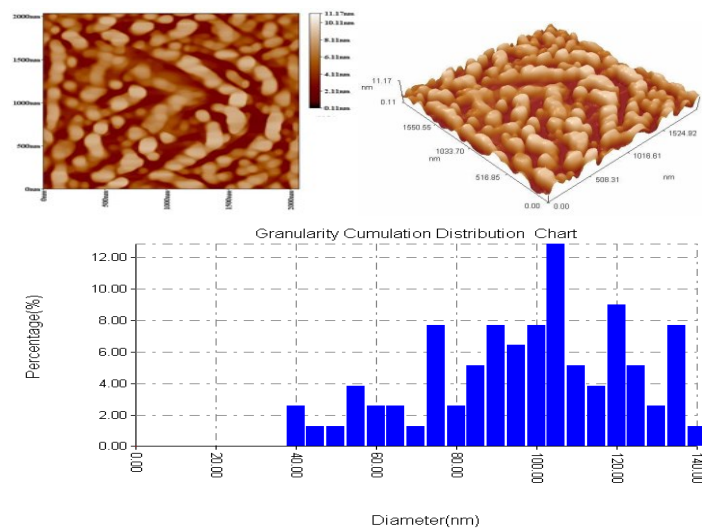


Figure 2: Typical AFM images of ZnO seed layer nanocrystals on Si using 20Mm of zinc acetate dehydrate, a) 2D image; b) 3D image; c) grain size distribution.

II. Crystal Structure Analysis

Figure 3 shows the XRD pattern for ZnO NWS grown on silicon (100) at 20mM using the hydrothermal method at 90°C for 2h. Three main strong peaks can be recognized at $2\theta = 32^\circ$, 34.6° , and 36.4° and indexed for (100), (002), and (101) reflection planes respectively. Other small peaks at $2\theta = 47.6$, 56.8 are indexed for (102) and (110) reflection planes respectively. These results are consistent with the standard data issued by JCPDS#36-1451. The strong diffraction peak of (002) indicates that the ZnO NRs were grown along with the c-axis orientation.

The crystallite size (D) was calculated using Sherrer's formula [38]:

$$D = 0.9\lambda / \beta \cos \theta \quad (1)$$

Where λ , β , and Θ are the wavelength (1.5406 Å), full width half maximum (FWHM), and Bragg's angle. The calculated average crystallite size for ZnO NRs was 25nm for [100], [002], and [101] directions. The lattice parameters of the hexagonal structure of ZnO NRs were also calculated using the formulas [36]:

$$A = (1/3)^{1/2} \lambda / \sin \Theta \quad (2)$$

$$c = \lambda / \sin \Theta \quad (3)$$

The calculated values of the lattice parameters of ZnO NRs are $a=3.2280\text{nm}$ $c=5.1767\text{nm}$. These results are consistent with the values of the Joint Committee on Powder Diffraction Standards [JCPDS# 36-1451].

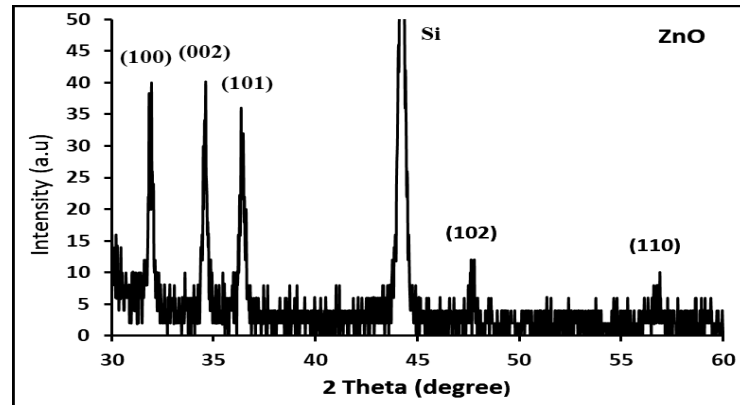


Figure 3 : XRD pattern of ZnO NRs grown hydrothermally on Si (100) with seed layer concentration of 20mM, 2h, 90°C.

III. Scanning Electron Microscope (SEM) Analysis

The morphology of the hydrothermally synthesized ZnO NRs at 20Mm seed layer concentration, 90°C, and for 2h was characterized via a scanning electron microscope (SEM). Figure 4 shows the SEM images at high and low magnifications. It was observed from Fig.4a a large area of ZnO nanorods agglomerated in a shape similar to flower-like nanorods. This shape was formed during the growth process from every single nuclei of ZnO seed nanoparticle and a joined group of nanorods leading to the formation of such flower-like. The average size of these micro flowers is about 5 μm as shown in Fig. 4b. The measured diameters of such nanorods and its length are about 80-100nm and 1 μm respectively. This gives an aspect ratio (rod length/diameter= L/D) value of 10. The small nanosize rod diameter is quite sensitive for gas sensor applications because of its large surface area.

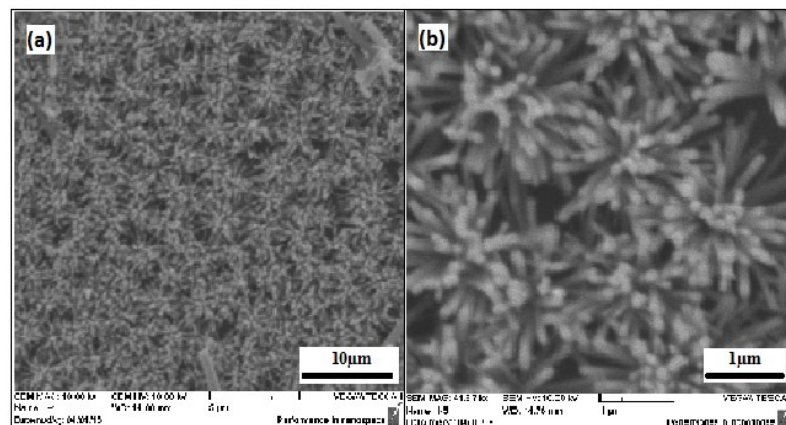


Figure 4: SEM images of hydrothermally synthesized ZnO NRs (Flower-like) on the silicon substrate.

IV. Energy –Dispersive X-ray Spectroscopy (EDS) Analysis

The synthesized and annealed ZnO nanostructure sample was analysed via EDS in order to investigate the chemical composition and the impurity of the products. The EDS spectrum is shown in Fig.5. The observed peaks of energy located in the range of 0-10keV are corresponding to the oxygen and zinc elements as indicated in the spectrum. The highest peak is corresponding to the Si substrate. It is clearly observed that the chemical composition is only zinc and oxygen elements. This means that our product is purely ZnO nanostructures with no other impurity found. Thus the EDS analysis confirms the purity of the samples. Thus the high purity obtained by the EDS analysis was supported by the previous XRD analysis. The atomic concentration of O and Zn are 59.59 and 40.43 respectively. It is confirmed the formation of ZnO NRs with a slightly rich of oxygen. In addition, the obtained values are quite consistent with the reported finding [39].

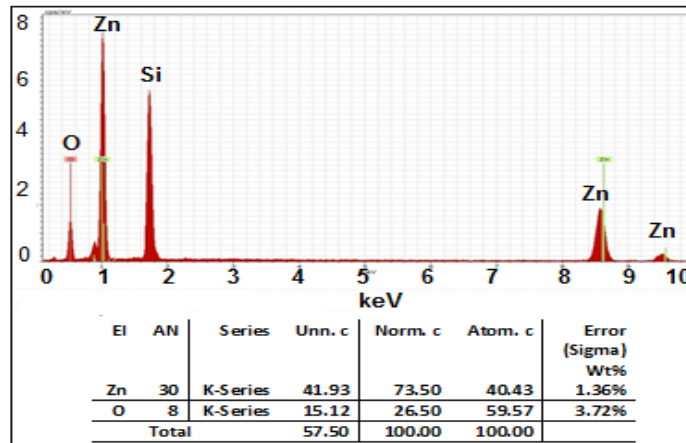


Figure 5: EDS of ZnO NRs on Si substrate.

4. OPTICAL PROPERTIES OF ZNO NRs

The absorbance (Fig. 5) of the ZnO NRs film was measured in the wavelength range 300–1100 nm. The film show a low absorbance (lower than 0.5) for the wavelengths higher than 500nm. This is corresponding to transmittance higher than 30% in that range.

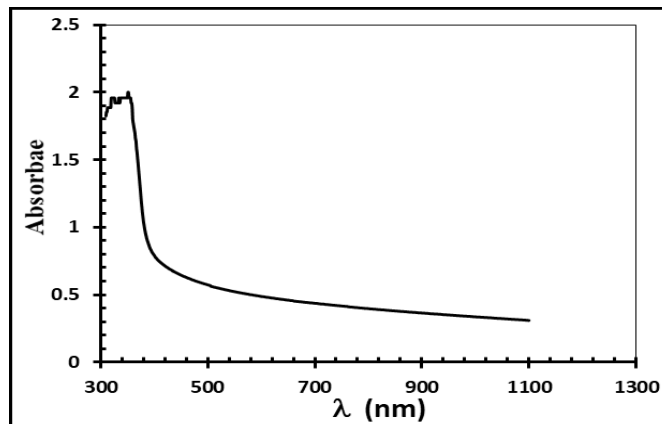


Figure 6: Absorbance of ZnO NRs film synthesized by the hydrothermal method.

Tauc's plot is normally used to calculate the energy bandgap for semiconducting thin films. This is given by the relationship between the photon energy and the absorption coefficient. For allowed direct transition Tauc's plot can be presented using the following equation.

$$\alpha h\nu = (h\nu - E_g)^{1/2} \quad (4)$$

Equation (4) says that if we plot against then we obtain a straight line at the band edge where the extrapolation of that portion intersects with at (mathematically at the intersection point). From Fig. 6

the band gap of ZnO NRs was found to be 3.2 eV. This value is comparable to what is reported for ZnO NRs prepared by aerosol assisted chemical vapor deposition [40] and ZnO films prepared by spray pyrolysis [41].

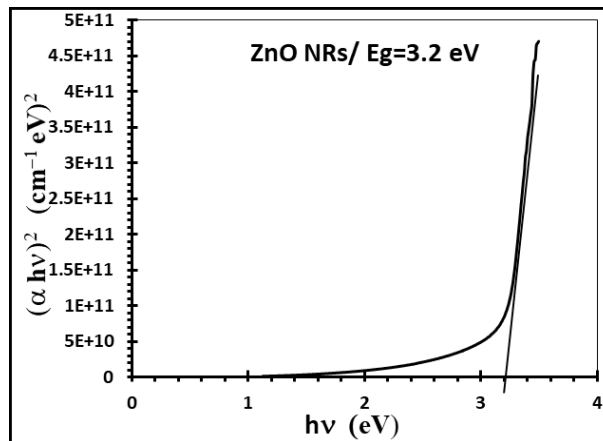


Figure 7: Tauc's plot for a ZnO NRs film synthesized by the hydrothermal method.

5. THERMAL AND ELECTRICAL MEASUREMENTS

The new homemade thermal and electrical measurement stage with temperature controller and shown in Fig. 7 was designed and manufactured in the laboratory. The resistance versus temperature of the sample was measured via an accurate digital electrometer (Keithley 616) and the programmable digital temperature controller respectively. The temperature varied from 25°C-200°C. This resistance variation against temperature is shown in Fig. 8. It was observed the decrease of the resistance when the temperature increased. This confirms the behavior of semiconductor material.

I Activation energy calculation

It is well known that the activation energy can be deduced from the resistance versus temperature curve obtained in Fig.8. The resistance as a function of temperature for semiconductor material is described by this relation [42]:

$$R=R_0 \exp (-E_a/KT) \tag{5}$$

Where R, R₀ , T, and k are the resistance at temperature T, the initial resistance, temperature, and the Boltzmann constant respectively. The resistance related to the conductivity (σ) through this formula:

$$R=L/A \sigma \text{ and so } = R_0L/A \sigma_0 \tag{6}$$

Where σ, σ₀ , and A are the conductivity at temperature T, initial conductivity and the cross-sectional area of the sample. So, by substitute Eq.2 in Eq1 to obtain:

$$\sigma = \sigma_0 \exp (-E_a/KT) \tag{7}$$

Taking the ln of both sides of Eq.3 to result:

$$\ln \sigma = \ln \sigma_0 - E_a/kT \tag{8}$$

The plot of ln σ on the y-axis and 1000/T (K-1) on the x-axis. This plot is shown in Fig. 9. The slope of the curve will equal to Ea/k, so the deduced activation energy of the ZnO NRs film is Ea=0.0578eV. This value of the activation energy is quite small which means that it will require small energy for the transition of electrons from the depletion region caused by the adsorbed oxygen atoms to the conduction band. This property could enhance gas sensor performance.



Figure 8: Photograph represents a home-made thermal and electrical measurement stage.

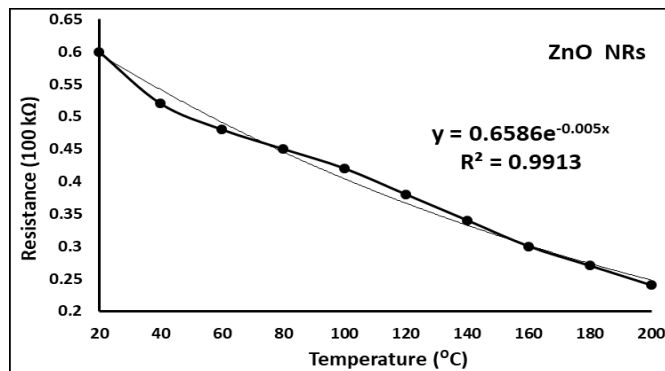


Figure 9: Resistance variation versus temperature of ZnO NRs film.

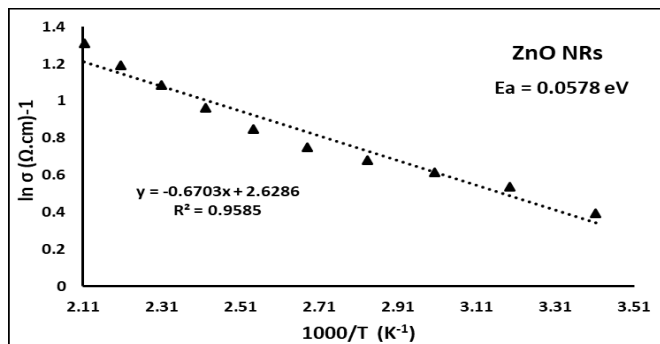


Figure 10: Ln σ versus 1000/T (K-1) plot of ZnO NRs film.

6. GAS SENSOR FABRICATION

Figure 11 shows schematically for the ZnO NWs gas sensor device. The silicon (100) was oxidized to SiO₂ film under air in the tube furnace at 1000C [43]. Aluminum electrodes in contact were evaporated on top of the surface of the nanowires. These are connected to a copper wire using a silver paste for measurements.

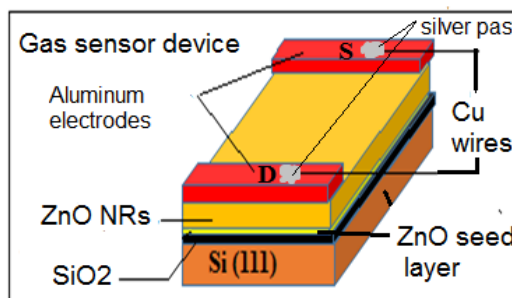


Figure 11: Schematic of a gas sensor device based on ZnO NRs.

I. I-V Characteristics

The I-V characteristics measured in Fig.11 show a linear relationship and it confirms a good ohmic contact between the ZnO and Al electrodes. This behavior indicates a good ohmic contact between the Al metal and the ZnO semiconductor. This property quite benefits for the sensor measurements where the sensitivity of gas sensors can be maximized for the metal-semiconductor junction [44].

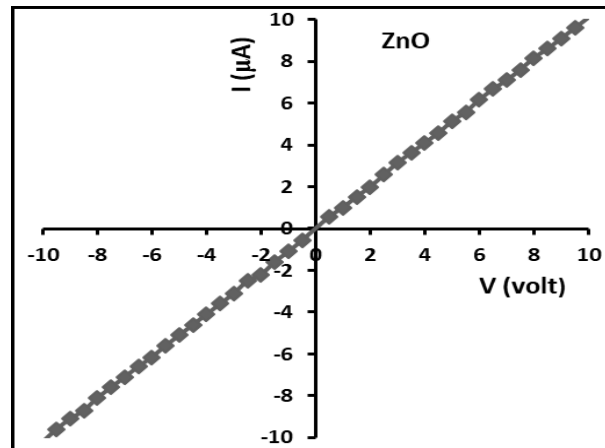


Figure 12: I-V characteristics for ZnO NRs /SiO₂/Si (100), hydrothermally synthesized at a seed layer concentration of 20mM.

II. Gas Sensor Performance

A. Experimental Calibration of Gas Sensing System

The new homemade gas sensor system is shown in Fig. 12 was designed, constructed, and manufactured in the laboratory. This system consists of the main gas chamber, rotary pump to pump, temperature reader, multimeter- Fluka, variable transformer (Variac), and hot plate. The ethanol liquid is heated by the hot plate to about 80C, evaporate the injected liquid. The concentration (C) of the ethanol was calculated using the formula [45]:

$$C \text{ (ppm)} = [V_l \text{ (ml)} / V_c \text{ (ml)}] * 10^{-6} \quad (9)$$

Where V_l and V_c are the volumes of the ethanol liquid and chamber used.

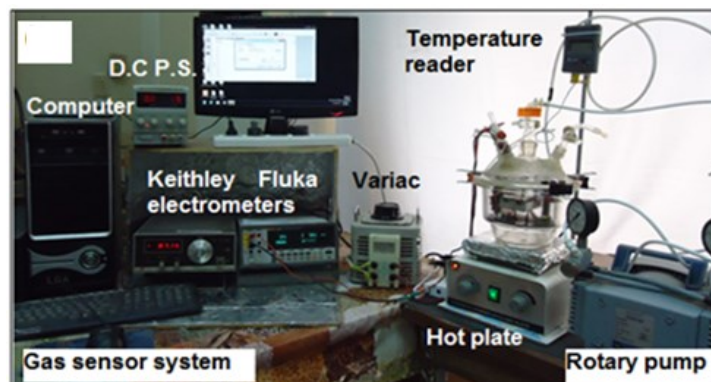


Figure 13: Photograph of the home-made gas sensor system; (a) complete setup; (b) Measurement stage; and (c) Glass reaction chamber.

This whole gas sensor system was tested and calibrated using ethanol vapor at 25°C and 200°C and at a concentration of 500ppm. These experiments were conducted at room temperature and ambient air.

Here in the first set experiment (denoted by RUN1) when the selected sample was fixed on the measurement stage inside the reaction chamber. The resistance of the air was firstly measured under air equilibrium. Then, a certain amount of liquid ethanol was calculated to obtain an equivalent to the

concentration of 500ppm of ethanol vapor. This concentration was injected through a rubber diaphragm to a 2 liter of glass dissector as a reaction chamber as shown in Fig.12c .

The resistance versus time was measured via an accurate digital multimeter (Fluka 8846A). Figure 13a demonstrates the variation of resistance versus time. It shows that this resistance is decreased against time until it reaches a stable value, then it increased to the original value. This calibration curve is called a resistance response which confirms the behavior of the n-type ZnO semiconductor towards ethanol vapor as a reducing agent .

The sensor properties can be deduced from this main curve shown in figure 14a such as relative response (S %), the response time (tresp.), recovery time (trec.), and the sensitivity (S%/1ppm). The sensitivity was calculated using the relation [46]:

$$S=[(R_a-R_g)/R_a] \times 100\% \quad (10)$$

To confirm the reliability of our experimental calibration results, so, the second set of the experiment (denoted by RUN 2) was conducted under similar conditions and on the same sample. The resistance versus time and its sensitivity curves are shown in Fig. 13 c and d respectively. They successfully confirm the previous results of Fig.13a and b. Table 1 demonstrates a quite acceptable sensor measurement properties using the newly designed and manufactured gas sensor system.

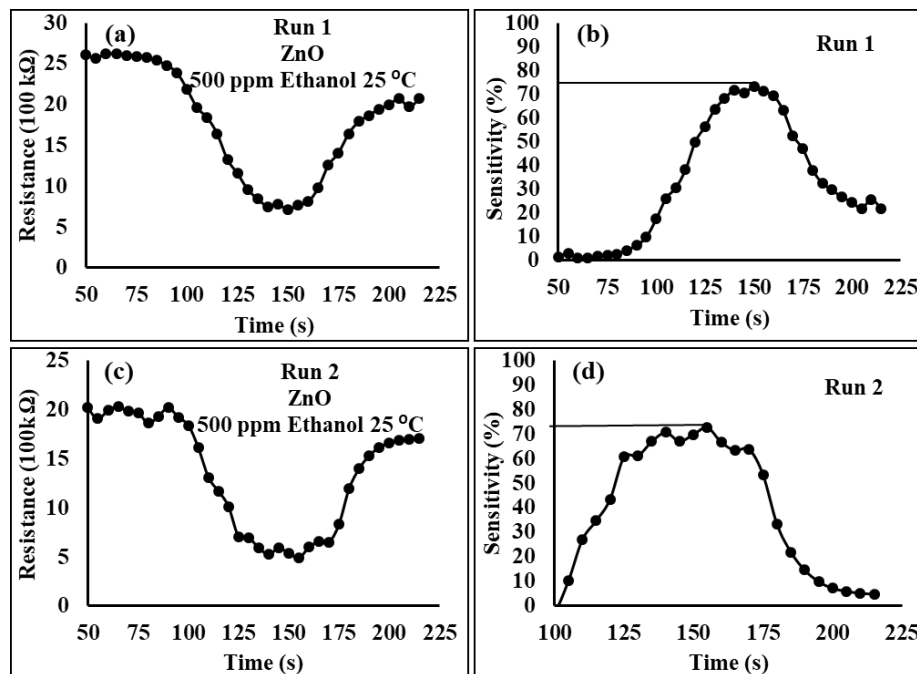


Figure 14: Experimental calibration curves (RUN 1a and b) and (RUN 2 c and d) for ZnO NRs sensing film towards 500ppm of ethanol vapor at 25°C

TABLE I: Summarizing the experimental calibration results of the ZnO gas sensor under test

Run No	Response time (sec.)	Recovery time (sec.)	Sensitivity (%)
1	45	65	73%
2	40	70	72%
Average values	42.5±2.5	67.5±2.5	72.5%±0.5%

III. Gas Sensor Properties

The gas sensor properties of ZnO NRs film on the silicon substrate, hydrothermally synthesized with seed layer concentration of 20 mM were executed using a laboratory homemade gas sensor system shown in Fig. 12a. The sensor measurements were conducted with ethanol vapor at 500 ppm of gas concentration. The sensing measurements were conducted at room temperature and 200°C.

Firstly, the resistance of the ZnO NRs film was measured as a function of time at ambient air. Then a certain concentration of ethanol liquid was injected through a rubber diaphragm into the preheated bottom of the reaction chamber. The liquid is evaporated inside the chamber to create vapor when reaching the equilibrium condition. Secondly, the resistance in the presence of ethanol vapor was measured versus time. It was observed that the resistance was decreasing under the exposure of ethanol vapor. This due to the reducing behavior of the ethanol as reducing gas and confirms the n-type semiconducting identity of the hydrothermally synthesized ZnO NRs.

Figure 14a represents the measured resistance versus time of ZnO NRs film on silicon towards 500ppm of ethanol vapor at 25°C and 200°C. It is observed that the minimum resistance is decreased when the temperature increased. The response and recovery time values were calculated from Fig. 14a. These values are shown in Table 2. The sensitivity versus time at 25°C and 200°C is shown in Fig. 14b. It is found that the sensitivity increased from 60% to 70% when the substrate temperature increased from 25°C to 200°C. These results are found to be consistent with the reported data in other literature [47].

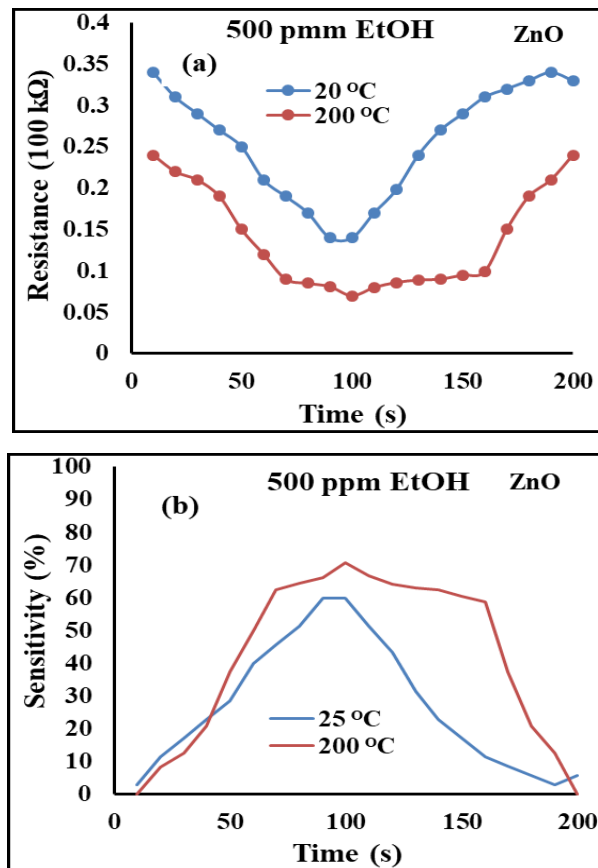


Figure 15: Typical ZnO NRs gas sensor properties measured at a concentration of 20mM and at substrate temperatures of 25 and 200°C; (a) Resistance versus time, (b) Sensitivity (S%) versus time.

TABLE II: Summarizing the sensor properties of ZnO NRs

Temperature (°C)	Response time (sec.)	Recovery time (sec.)	Sensitivity= Ra-Rg/Ra(%)	Sensitivity= Ra/Rg	Ref.
25	80	80	60%	2.3	[45]
200	60	50	70%	3.3	

7. CONCLUSION

In this conclusion, one dimensional (1D) zinc oxide (ZnO) flower-like nanorods were successfully achieved via low-temperature hydrothermal technique at ambient atmosphere. The analysis via XRD and EDS was confirmed the formation of high purity hexagonal Wurtzite crystal structure of ZnO NRs. The SEM images visualizing the formation of flower-like nanorods with a

micro-size structure. The ZnO rod diameter measured from the SEM image was consistent with the AFM analysis. A new gas sensor system was successfully designed, constructed, calibrated and used for gas sensor fabrication devices towards ethanol vapor at 25°C and 200°C. So, the main finding of this gas sensor results is the increase of the sensitivity as the temperature increased from 25°C to 200°C. This sensitivity enhancement is due to the increase of chemisorbed species on the sensor surface at high temperature.

Acknowledgement

I'm sincerely grateful to the University of Technology and the head of the Applied Science research unit (ASRU) and all the staff for this great opportunity that they gave me in order to finish this work.

REFERENCES

- [1] M. H. Huang, S. Mao, H. Feick, H. Yan, Y. Wu, H. Kind, E. Weber, R. Russo, and P. Yang, "Room-temperature ultraviolet nanowire nanolasers," *Science*, Vol. 292, Issue 5523, pp. 1897-1899, 2001.
- [2] J. Zhong, A. H. Kitai, P. Mascher, and W. Puff, "Effect of substrate temperature on the growth and luminescence properties of ZnO nanostructures," *J. Electrochem. Soc.* Vol.140, pp.3644- 3649, 1993.
- [3] N. Beermann, L. Vayssieres, S.-E. Lindquist, and A. Hagfeldt, "Photoelectrochemical studies of oriented nanorod thin films of Hematite," *J. Electrochem. Soc.* Vol.147, pp.2456- 2461, 2000.
- [4] N. Yamazoe, "New approaches for improving semiconductor gas sensors," *Sens. Actuators B: Chem.*, Vol. 5, pp. 7-19, 1991.
- [5] M. Law, L.E. Greene, J.C. Johnson, R. Saykally, and P. Yang, "Nanowire dye-sensitized solar cells," *Nat. Mater.* Vol.4, pp.455- 459, 2005.
- [6] T. Yoshida, K. Terada, D. Schlettwein, T. Oekermann, T. Sugiura, and H. Minoura, "Electrochemical and photoelectrochemical properties of organic semiconductors - dye-sensitization in nanostructured hybrid Materials," *Adv. Mater.* Vol.12, pp. 1214- 1217, 2000 .
- [7] E. Hosono, S. Fujihara, I. Honma, and H. Zhou, "The fabrication of an upright-standing zinc oxide nanosheet for use in dye-sensitized solar cells," *Adv. Mater.* Vol.17, pp.2091- 2094, 2005.
- [8] L.E. Greene, M. Law, D.H.Tan, M. Montano, J. Goldberger, G. Somorjai, and P. Yang, "ZnO nanowire/p-GaN heterojunction LEDs," *Nano. Lett.* Vol.5, pp.1231- 1236, 2005.
- [9] J.B. Baxter, and E.S. Aydil, "Nanowire-based dye-sensitized solar cells," *Appl. Phys. Lett.* Vol.86, pp. 053114(1-2), 2005.
- [10] S. Narasimmana, L. Balakrishnanb, S.R.Meherb,R. Sivacoumara and Z.C.Alexa, "ZnO Nanoparticles based Fiber Optic Gas Sensor," *AIP Conf. Proc.* Vol. 1731, pp. 050052(1-3), 2016.
- [11] R. Kumar, O. Al-Dossary, G. Kumar, and A. Umar, "Zinc Oxide Nanostructures for NO₂ Gas-Sensor Applications: A Review," *Nano-Micro Lett.* Vol. 7, pp. 97-120, 2015.
- [12] H. S. Hassan , A.B. Kashyout , I. Morsi , A.A.A. Nasser , I. Ali., "Synthesis, characterization and fabrication of gas sensor devices using ZnO and ZnO:In nanomaterials," *Beni-Suef University Journal of Basic and Applied Sciences*, pp.1-6, 2014.
- [13] W.U. Huynh, J.J. Dittmer, and A.P. Alivisatos, "Investigation of properties of ZnO nanorod structures by chemical vapor deposition," *Science* Vol.295, pp.2425- 2427, 2002.
- [14] T. Stubinger, and W. Brutting, "Exciton diffusion and optical interference in organic donor-acceptor photovoltaic cells," *J. Appl. Phys.* Vol.90, pp.3632- 3641, 2001.
- [15] C.J. Brabec, N.S. Sariciftci, and J.C. Hummelen, "Origin of the open circuit voltage of plastic solar cells," *Adv. Funct. Mater.* Vol.11, pp.15- 26, 2001.
- [16] B. Pradhan, A. Bandyopadhyay, and A. J Pal, "Functionalized carbon nanotubes in donor/acceptor-type photovoltaic devices," *Appl. Phys.Lett.* Vol.88, pp. 093106(1-3), 2006.
- [17] M. H. Huang, Y.Wu, H. Feick, N. Tran, E.Weber, and P. Yang, "Catalytic growth of zinc oxide nanowires by vapor transport," *Adv. Mater.* Vol.13, pp.113- 116, 2001 .

- [18] A. D Faisal, "Optimization of CVD parameters for long ZnO NWs grown on ITO/glass substrate," *Bull. Mater. Sci.*, Vol. 39, No. 7, pp. 1635–1643, 2016 .
- [19] X. Liu, X. Wu, H. Cao, and R. P. H. Chang, "Growth mechanism and properties of ZnO nanorods synthesized by plasma-enhanced chemical vapor deposition," *J. Appl. Phys.* 95, 3141–3147, 2004 .
- [20] Y.C. Kong, D.P. Yu, B. Zhang, W. Fang, and S.Q. Feng, "Ultraviolet-emitting ZnO nanowires synthesized by a physical vapor deposition approach," *Appl. Phys.Lett.* Vol.78, pp.407- 409, 2001.
- [21] J.-J. Wu, and S.-C. Liu, "Low-temperature and catalyst-free synthesis of well-aligned ZnO nanorods on Si (100)," *Adv. Mater.* Vol.14, pp.215-218, 2002.
- [22] J.-J. Wu, and S.-C. Liu, "Catalyst-free growth and characterization of ZnO nanorods," *J. Phys. Chem. B* Vol.106, pp.9546- 9551, 2002.
- [23] J. Zhang, L. Sun, H. Pan, C. Liao, and C. Yan, "ZnO nanowires fabricated by a convenient route," *New J. Chem.* Vol.26, pp. 33-34, 2002.
- [24] Y. Li, G.W. Meng, L.D. Zhang, and F. Phillipp, "Ordered semiconductor ZnO nanowire arrays and their photoluminescence properties" *Appl. Phys. Lett.* Vol.76, pp. 2011, 2000.
- [25] L. Wang, Y. Kang, X. Liu, S. Zhang, W. Huang, and S. Wang, "ZnO nanorod gas sensor for ethanol detection", *Sens. Actuators B: Chem.*, Vol. 162, pp. 237– 243, 2012.
- [26] D. Zhang, S. Chava, C. Berven, S.K. Lee, and R. Devitt, V. Katkanant, "Experimental study of electrical properties of ZnO nanowire random networks for gas sensing and electronic devices," *Appl. Phys. A* 100, pp. 145–150, 2010.
- [27] C.M. Chang, M.H. Hon, and I.C. Leu, "Preparation of ZnO nanorod arrays with tailored defect-related characteristics and their effect on the ethanol gas sensing performance, " *Sens. Actuators B* Vol. 151, pp. 15–20, 2010.
- [28] J.Q. Xu, Y.P. Chen, D.Y. Chen, and J.N. Shen, "Hydrothermal synthesis and gas sensing characters of ZnO nanorods, " *Sens. Actuators B* Vol. 113, pp. 526–531, 2006.
- [29] L. Li, H.Q. Yang, H. Zhao, J. Yu, J.H. Ma, L.J. An, and X.W. Wang, "Hydrothermal synthesis and gas sensing properties of single-crystalline ultralong ZnO nanowires, " *Appl. Phys. A* 98, pp. 635–641, 2010.
- [30] J. Kim, and K. Yong, "Mechanism study of ZnO nanorod-bundle sensors for H₂S gas sensing, " *J. Phys. Chem. C* 115, pp. 7218–7224, 2011.
- [31] Y.Y. Zhang, and J. Mu, "Controllable synthesis of flower- and rod-like ZnO nanostructures by simply tuning the ratio of sodium hydroxide to zinc acetate, " *Nanotechnology* Vol. 18, pp. 1-6, 2007.
- [32] X.F. Chu, D.L. Jiang, B.D. Aleksandra, and H.L. Yu, "Gas-sensing properties of thick film based on ZnO nano-tetrapods, " *Chem. Phys. Lett.* Vol. 401, pp. 426–429, 2005.
- [33] R.s B. Kale, Y. –J. Hsu, Y.-F. Lin, and S.-Y. Lu, "Hydrothermal synthesis, characterization and photoluminescence study of single crystalline hexagonal ZnO nanorods with three-dimensional flower-like microstructures, " *Superlatt. Microstr.* Vol. 69, pp.239-252, 2014.
- [34] A. D. Faisal, "Influence of seed layer on morphology and structure of ZnO nanowires synthesized on silicon via hydrothermal method," *Al-Mustansiriyah J. of Sci.*, Vol. 27, No 3, pp. 62-67, 2016.
- [35] J. Fan, T. Li and H. Heng, "Hydrothermal growth of ZnO nanoflowers and their photocatalyst application, " *Bull. Mater. Sci.* Vol.39 No. 1, pp.19-26, 2016.
- [36] A. D. Faisal, "Synthesis of ZnO comb-like nanostructures for high sensitivity H₂S gas sensor fabrication at room temperature," *Bull. Mater. Sci.*, Vol. 40, No. 6, Oct. 2017, pp. 1061–1068.
- [37] D. Pellegrino, G. Franzò, V. Strano, S. Mirabella and E. Bruno, "Improved synthesis of ZnO nanowalls: effects of chemical bath deposition time and annealing temperature," *Chemosensors*, Vol. 7, Issue 18; pp.1-10, 2019 .
- [38] E. Darezereshki, M. Ranjbar, and F. Bakhtiari, "One-step synthesis of maghemite (γ -Fe₂O₃) nanoparticles by a wet chemical method, " *J. Alloys Compounds*, Vol. 502, pp.257-260, 2010 .
- [39] S. Brintha and M. Ajitha, "Synthesis and characterization of ZnO nanoparticles via aqueous solution, sol-gel and hydrothermal methods, " *IOSR J. Appl. Chem.*, Vol. 8, Issue 11, pp.66-72, 2015.

- [40] A. S. Trevizo, P. Madrid, P. Ruiz, W. Flores, and M. Miki-Yoshida, "Optical Band Gap Estimation of ZnO Nanorods," *Mat. Res.* Vol.19, pp. 33-38, 2016 .
- [41] V. R. Shinde, T. P. Gujar, C.D. Lokhande, R.S. Mane, and S.-H. Han, "Mn doped and undoped ZnO films: A comparative structural, optical and electrical properties study," *Mater. Chem. Phys.*, Vol. 96, pp. 326–330, 2006.
- [42] G. Frank and H. Kostlin, "Electrical Properties and Defect Model of Tin-Doped Indium Oxide Layers," *Appl. Phys. A*, 27, pp.197-206, 1982.
- [43] Lin CH. (2008) Oxidation (of Silicon). In: Li D. (eds) *Encyclopedia of Microfluidics and Nanofluidics*, Springer, Boston, MA .https://doi.org/10.1007/978-0-387-48998-8_1173
- [44] S. Santra, P.K. Guha, S.Z.Ali, P.Hiralal, H.E. Unalan, J. A. Covington, G.A.J. Amaratunga, W.I. Milne, J.W.Gardner, and F. Udrea, "ZnO nanowires grown on SOI CMOS substrate for ethanol sensing," *Sens. Actuators B: Chem.*, Vol. 146, pp.559-565, 2010 .
- [45] N. Never, "Air Pollution Control Engineering," McGraw-HILL, Singapore 1995.
- [46] R. S. Andre, D. Kwak, Q. Dong, W. Zhong, D. S. Correa, L. H. C. Mattoso, and Y. Lei, "Sensitive and selective NH₃ monitoring at room temperature using ZnO ceramic nanofibers decorated with poly(styrene sulfonate)," *Sensors*, Vol. 18 Issue 1058, pp. 1-13, 2018.
- [47] M. Z. Ahmad , A. Z. Sade , K. Latham , J. Kita , R. Moos and W. Wlodarski, "Chemically synthesized one-dimensional zinc oxide nanorods ethanol sensing," *Sens. Actuators B: Chem.*, Vol. 187, pp. 295-300, 2013.